Quantitative analysis of the intraretinal layers and optic nerve head using ultra-high resolution optical coherence tomography

Yuhong Wang
Hong Jiang
Meixiao Shen
Byron L. Lam
Delia Cabrera DeBuc
Yufeng Ye
Ming Li
Aizhu Tao
Yilei Shao
Jianhua Wang

Quantitative analysis of the intraretinal layers and optic nerve head using ultra-high resolution optical coherence tomography

Yuhong Wang,[a,b] **Hong Jiang,**[b,c] **Meixiao Shen,**[a,b] **Byron L. Lam,**[b] **Delia Cabrera DeBuc,**[b] **Yufeng Ye,**[d,b] **Ming Li,**[a,b] **Aizhu Tao,**[a,b] **Yilei Shao,**[a,b] **and Jianhua Wang**[b]

[a]Wenzhou Medical College, School of Ophthalmology and Optometry, Wenzhou, Zhejiang, China
[b]University of Miami, Bascom Palmer Eye Institute, Miami, Florida
[c]University of Miami, Neurology, Miami, Florida
[d]Hangzhou First People's Hospital, Hangzhou, China

Abstract. This study is designed to test the repeatability of the quantitative analysis of intraretinal layer thickness and cup-disc ratio of the optic nerve head using ultra-high resolution optical coherence tomography (UHR-OCT). Group A, containing 23 eyes of 12 healthy subjects, was imaged twice and group B, containing eight eyes of four subjects, was imaged three times. Intraretinal layers were segmented manually and the cup-to-disc ratio of the optic nerve head was analyzed. Custom-built automatic segmentation software was also used to segment a set of images for comparison. A total of nine intraretinal layers were visualized and extracted manually. With group A, the central foveal thickness was 186.4 ± 15.9 μm (mean $\pm$ SD). The average retinal thickness was 296.4 ± 21.3 μm. The best repeatability, obtained when two repeated scans were taken, was obtained for the outer nuclear layer followed by the ganglion cell layer, the inner nuclear layer, the retinal nerve fiber layer and the worst was obtained for the outer segment. The intraclass correlation ranged from 0.824 to 0.997. The coefficients of repeatability ranged from 3.24 to 18.3 μm, corresponding to 1.47% to 26.20%. With group B, high interclass correlations were found and the automatic segmentation results were compatible with the manual results. Our results indicated that more retinal features might be imageable using UHR-OCT. © *2012 Society of Photo-Optical Instrumentation Engineers (SPIE)*. [DOI: 10.1117/1.JBO.17.6.066013]

Keywords: ultra-high resolution optical coherence tomography; spectral domain; retinal segment; optic nerve head; quantitative analysis; segmentation, image processing.

Paper 11588 received Oct. 8, 2011; revised manuscript received Apr. 18, 2012; accepted for publication Apr. 20, 2012; published online Jun. 4, 2012.

1 Introduction

Optical coherence tomography (OCT) has a history going back more than 20 years in ophthalmic imaging.[1] Recent advances in ultra-high resolution spectral domain OCT make this imaging modality more useful in research and patient care.[2] OCT can provide high-resolution cross-sectional images of the retina to aid in identifying, monitoring, and quantitatively assessing ocular diseases[1,3,4] and ocular manifestations of diseases in the central nervous system disorders, such as multiple sclerosis[5,6] and stroke. Most of commercially available OCT devices have an approximately axial resolution of 5 μm and are limited to a few segmented intraretinal layers, although the segmentation is mostly automatic.[2,7] These commercial devices have become an important part of ophthalmic patient care and the conduct of clinical trials. The general trend appears to be toward imaging more details of ocular structures up to the cellular level, allowing earlier detection and more precise follow-up of disease progression. Ultra-high resolution OCT (UHR-OCT) enables better visualization of intraretinal structures, which had previously only been possible with histopathology.[8,9] The goal of the present study was to explore whether more retinal features might be measured and imageable with greater details by using UHR-OCT. We tested the repeatability of the quantitative analysis used to measure intraretinal layer thickness and cup-disc ratio of the optic nerve head using UHR-OCT.

2 Materials and Methods

The study was approved by the Institutional Review Board at the University of Miami. All participants provided written informed consent and were treated according to the tenets set forth in the Declaration of Helsinki. In group A, 23 eyes from 12 healthy subjects with a mean age of 34 years (range from 26 to 46 years) were recruited for this study. In addition, eight eyes of four healthy subjects (group B) were used as a subset for testing interclass repeatability and comparing manual and automatic segmentation methods. Inclusion criteria included best-corrected visual acuity of 20/20 or better, no history of ocular or systematic disease, no history of ocular surgery or laser, and normal appearance of the macula and optic disc. All subjects underwent visual acuity testing, refraction and complete slit-lamp biomicroscopic examination and ophthalmoscopic examination.

The UHR-OCT was custom developed based on our previous UHR-OCT device.[10,11] With this version, a broadband light source (T870-HP, Superlum Diodes Ltd., Moscow, Russia) with a center wavelength of 870 nm and a bandwidth of 188 nm was used with a specially designed spectrometer.[12]

Address all correspondence to: Hong Jiang, University of Miami, Bascom Palmer Eye Institute, Miller School of Medicine, 1638 NW 10th Avenue, McKnight Building—Room 202A, Miami, Florida 33136. Tel: +1 305 4825010; E-mail: hjiang@med.miami.edu

Similar to our previous UHR-OCT system, a charge-coupled device camera with a scan speed set to 24,000 A-scans per second was used. The calibrated axial resolution was 2.2 μm in tissue (refractive index = 1.38).[12] In the sample arm, the light delivery system was driven by an X-Y galvanometer scanner, which was mounted on a standard slit-lamp. A computer controlled fixation target was provided for facilitating the alignment. A co-axial video camera incorporated into the slit-lamp optics served as a view finder. The incident light power was set to 750 μW, which is well below the safety standard according to the American National Standards Institute (ANSI Z136.1-2000). To image the retina, an ocular lens (60D, Volk Optical, Mentor, OH, USA) was used.[12,13] The calibration of the scan depth was described in our previous study.[14] Briefly, a custom apparatus was used. A water chamber with known thickness was used and OCT scans were performed through a lens and 25 mm water tube before reached the chamber. OCT images of the chamber thickness were processed to obtained numbers of pixels between two boundaries that formed the chamber. The thickness in the water (n = 1.333) was obtained. The calibrated scan depth was 1.48 mm in air. To calibrate the scan width on the retina, a model eye (OEMI-7, Ocular Instruments, Bellevue, WA), with a grid implanted on the fundus, was used to calibrate the scan width. Each lattice is 1 mm in width. A horizontal B-scan was performed crossing the grid, and the pixel numbers

corresponding to one lattice were acquired. In this study, the calibrated scan width was set to be six millimeters. In addition, a time-domain commercial OCT (StratusOCT, Carl Zeiss Meditec, Dublin, CA) was used to image the macula in one healthy subject for comparison [Fig. 1(a)].

All measurements with UHR-OCT were taken without pupil dilation in a semi-dark room. During OCT imaging, the subject was asked to gaze at the internal green fixation target. A line scan was used to scan the macula with a dataset of 2048 (depth) × 2048 (transverse) pixels [see Fig. 1(b) and 1(c)]. Only images with foveal light reflex (macular image) were processed for measurement [Fig. 1(c)]. A tridimensional scan of a 6 × 6 mm^2 area centered on the optic disc [Fig. 2(a)] was scanned with a 2048 (depth) × 512 (transverse) × 128 (frames) dataset. During processing, the horizontal B-scan with 2048 (depth) × 512 (transverse) pixels crossing the disc center [Fig. 2(b)] was extracted, and the cup-disc ratio was analyzed [Fig. 2(c)]. The image was repeated if the fixation was unstable or if the subject blinked. In order to assess repeatability, two consecutive scans were taken for each eye of group A (i.e., 23 eyes of 12 subjects) under the same conditions by one examiner (YW). The subject was repositioned after each scan. In addition, in order to assess interclass repeatability and compare manual and automatic segmentation approaches, the scans were repeated three times in the same fashion to acquire the images
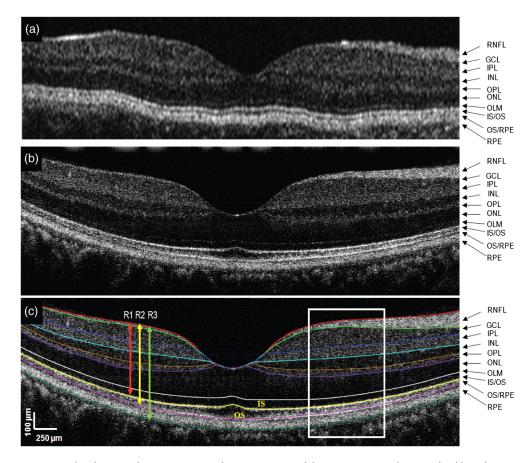

Fig. 1 Macular images acquired with a time-domain commercial OCT (Stratus) and the UHR-SD-OCT device. A healthy subject was imaged with the Stratus OCT (a). The macular image (b) of another healthy subject was imaged with the UHR-SD-OCT (2048 × 2048 pixels, 6-mm width) showing manual segmentation results (c) obtained with the custom-built software. The nine layers of the total retina are clearly distinguished: the retinal nerve fiber layer (RNFL), ganglion cell layer (GCL), inner plexiform layer (IPL), inner nuclear layer (INL), outer plexiform layer (OPL), outer nuclear layer (ONL), the photoreceptor inner segment (IS), the photoreceptor outer segment (OS), and the retinal pigment epithelium (RPE). The, outer limiting membrane (OLM); the junction inner and outer segment of photoreceptors (IS/OS); and the junction of the outer segments and RPE (OS/RPE) are also outlined. Retina 1 (R1), Retina 2 (R2) and Retina 3 (R3) are marked with vertical arrows.
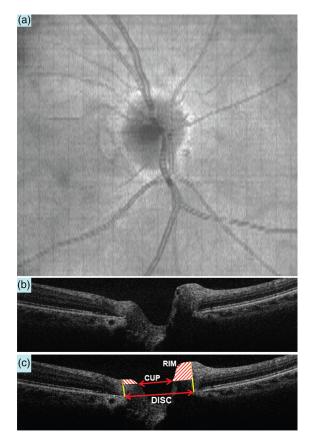
Fig. 2 A horizontal B-scan OCT image crossing the center of the optic nerve head disc was extracted from a 3D square scan ($512 \times 128 \times 2048$ pixels, 6×6 mm^2). (a) The *en face* view of the optic nerve head. The artery, vein, cup, and optic disc are clearly visualized. (b) B-scan OCT image. The cup and disc are clearly visible in the horizontal cross-sectional OCT image (512×2048 pixels). (c) The B-scan OCT image (512×2048 pixels) is marked to show the rim of the optic nerve and the cup-to-disc ratio (0.488).

Fig. 3 Automatic segmentation of the OCT image. The nasal half of the fovea (a) in a healthy subject was imaged with the UHR-SD-OCT device. The custom-built automatic segmentation software was used to process the image and intra-retinal layers were fully automatically segmented. The thickness of the layers averaged from the marked rectangular area (b) was used to compare with the results obtained manually. Five intraretinal layers were successfully segmented and distinguished as the retinal nerve fiber layer (RNFL), ganglion cell layer plus inner plexiform layer (GCL + IPL), inner nuclear layer (INL), outer plexiform layer (OPL) and outer nuclear layer (ONL). In general, minor segmentation errors were obtained for the IPL's inner border, outer border of the photoreceptor inner/outer segments (IS, OS), and the RPE's outer border. Therefore, only the GCL + IPL complex along with 4 additional intraretinal layers (RNFL, OPL, INL, and ONL) were considered in the comparison with manual segmentation.

centered at the fovea of group B [i.e., eight eyes of four subjects, see Fig. 3(a)].

All OCT images were exported and custom-built software was used for quantitative analysis of the thickness of intraretinal layers. The custom-built software, which has been described elsewhere,[15–18] was used to manually and automatically segment these layers. Because the manual segmentation is labor intensive and time consuming, a particular approach was used to outline the boundaries of these layers in a small area nasally from the fovea. Specifically, the operator manually marked the boundaries of each layer on both consecutive scans obtained from all eyes and the software calculated their corresponding thickness [see Fig. 1(c)]. A total of ten boundaries were graded in the macular OCT image.[19,20] The first hyperreflective layer below the outer limiting membrane (OLM) is the junctional complex of photoreceptor inner segment and outer segment (IS/OS junction). The hyporeflective band below this junction, which is clearly wider in the fovea, is attributed to the photoreceptor outer segment (OS). The hyporeflective band between the OLM and IS/OS junction is the photoreceptor inner segment (IS). The second hyperreflective layer below OLM corresponds to the outer segments interdigitating with the microvilli of the retinal pigment epithelium (RPE), which is the OS/RPE junction. The third hyperreflective layer, identified as the RPE, is probably due to a signal from the RPE cell bodies, although
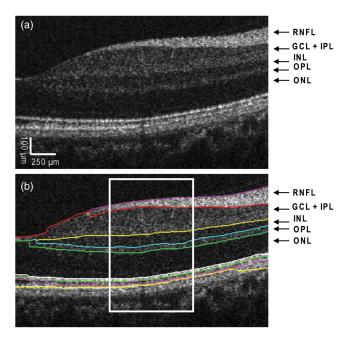
reflections from the choriocapillaris may also be included.[21–23] The ten boundaries segmented the retina into nine layers: the retinal nerve fiber layer (RNFL), the ganglion cell layer (GCL), the inner plexiform layer (IPL), the inner nuclear layer (INL), the outer plexiform layer (OPL), the outer nuclear layer (ONL), the photoreceptor inner segment (IS), the photoreceptor outer segment (OS), and the RPE. Because of different assumptions considered for the detection of the outer retinal boundary exist in the literature,[18] three retinal segments were used in the comparative analyses. Retina 1 was defined as the segment between the inner limiting membrane (ILM) and the intermediate of the IS/OS junction. Retina 2 was defined as the segment between the ILM and the intermediate of the OS/RPE junction. Retina 3 was defined as the segment between the ILM and the posterior boundary of the RPE. The thickness of these layers and segments were averaged from a 1-mm-long section located 1-mm nasal from the fovea (Figs. 1 and 3). In addition, we calculated the average thickness values at the foveal center for each retinal segment described above (Fovea 1, Fovea 2, and Fovea 3). Moreover, the cup and disc diameters were measured from the optic nerve head OCT image in order to calculate the cup-to-disc ratio (Fig. 2). The boundary of the optic disc was determined from each OCT image by the point at which the photoreceptor layer, RPE, and choriocapillaris terminate at the lamina cribrosa. The disc diameter was determined by measuring the distance between

the disc boundaries on opposite sides of the disc. The cup diameter were measured by constructing a line parallel to and offset anteriorly by 150 μm[24,25] to the line that defines the disc diameter.

Additionally, three graders independently graded the intraretinal boundaries by hand on a total of 24 images obtained after scanning the eight eyes in the subset three times. Our custom automatic segmentation software[15–18] was also used to automatically detect boundaries on OCT images from this subset. Segmentation errors were identified in all images by visual inspection, and a total of five automatically segmented layers [namely as RNFL, GCL + IPL complex, INL, OPL and ONL, Fig. 3(b)] without segmentation errors were selected from the subset (i.e. 24 images) and compared with the manual results.

A statistical analysis was performed using the software package SPSS version 16 (SPSS Inc., Chicago, Illinois). The methods outlined by Bland and Altman[26] were used for assessing the agreement between two measurements. The coefficients of repeatability (CR) and intraclass correlation coefficients (ICC) of intraretinal layer thickness and cup-to-disc ratio were calculated. The ICC was calculated on the basis of a two-way mixed model for analysis of variance (ANOVA) as proposed by Bartko and Carpenter.[27] The definition of coefficient of repeatability was based on those adopted by the International Organization for Standardization.[28,29] The CR was defined as two standard deviations of the difference between two measurements. Pearson correlation coefficient (r) was used to describe the interclass correlation among graders.

3 Results

A total of nine intraretinal layers were visualized [Fig. 1(b)] and manually extracted [Fig. 1(c)]. The OLM and OS/RPE junction were clearly visible, particularly, in the fovea. The intensity of the OLM gradually appeared more faded away from the fovea. With the group A, the central foveal thickness was 186.4 ± 15.9 μm (mean $\pm$ SD). The average total retinal thickness was 296.4 ± 21.3 μm. The thicknesses of the intraretinal layers ranged from 20.8 to 67.6 μm (Table 1). The best repeatability was obtained for the ONL followed by the GCL, INL, RNFL and the worst was obtained by the OS (Table 1). Retina 1 (assumption using the IS/OS as outer border) provided a much better repeatability when compared with Retina 2 and Retina 3. Retina 2 gave the worst repeatability. The ICC of these layers ranged from 0.824 to 0.997. The CR ranged from 3.24 to 18.3 μm, corresponding to 1.47 to 26.20%. The agreement between the two measurements for each layer and retinal segment was plotted using the Bland–Altman Plot (Fig. 4). With the group B, r ranged from 0.965 to 0.976 between each pair of the three graders and measurements from overall segmented layers (Figs. 5 and 6). CR ranged from 7.1 to 8.6 μm and CR% ranged from 20.0% to 24.2% from overall segmented layers. Between manual and automatic segmentation methods of these detected 5 intraretinal layers, r was 0.999 (Fig. 7).

4 Discussion

Imaging the retina in great detail is beneficial to monitor disease progression, not only for ocular diseases like glaucoma and macular degeneration but also for central nervous system conditions. For instance, the use of OCT has become an integral part of patient care to access macular conditions such as cystoid macular edema. The retina is also part of the central nervous system and is a readily accessible window to the brain for studying neurodegeneration and the distal effect of demyelination. Several investigators have identified OCT derived RNFL layer thinning in multiple sclerosis, which was found to correlate with white matter brain atrophy and RNFL thinning has been used as one of the biomarkers in clinical trials for evaluating the efficacy of new treatment.[30–32] Moreover, thinning of the ganglion cell complex in the inner retina was also found in eyes of multiple sclerosis patients regardless of previous optic neuritis using Stratus OCT (G. M., Somfai, et al., IOVS 2011;52: ARVO E-abstract 2999). Detailed visualization and quantification of more intraretinal layers in the OCT images obtained with high resolution OCT will improve the understanding of pathophysiology. For example, using high resolution OCT (Cirrus OCT), Saidha et al.[6] identified RNFL thinning and significant thinning of both the inner nuclear layer and outer nuclear layer in multiple sclerosis patients. In the present study, we explore whether more retinal features might be repeatably measured and imageable with greater details by using UHR-OCT. Specifically, the clinical applicability of our ultra-high resolution OCT in future clinical studies of retinal neurodegeneration was tested by examining the repeatability of the UHR-OCT system using both custom-built segmentation and manual segmentation methods.

Precise segmentation of the intraretinal layers is as important as the development of the hardware. With the advancement of the hardware in the era of spectral domain OCT, the axial resolution can be as high as 1 to 2 μm.[8,9,33–38] Wojtkowski et al. developed an ultra-high resolution OCT with a resolution of 2 μm for retinal scanning with a limited intraretinal layer segmentation.[39] Currently commercial OCT devices, including the Spectralis (Heidelberg Engineering, Dossenheim, Germany), Cirrus (Carl Zeiss Meditec, Dublin, CA, USA), RTVue-100 (Optovue, Meridianville, AL,. USA) and others, have achieved approximately 5 μm axial resolution.[40–42] There are two commercially available ultra-high resolution OCT devices with an axial resolution of approximately 3 μm, including the Biotigen SD-OCT (Bioptigen Inc., Research Triangle Park, NC)[43,44] and the Copernicus HR SOCT (Optopol Technology SA, Zawiercie, Poland).[45] With these devices, the quality of retinal OCT images have been dramatically improved compared to time-domain OCT devices, such as the Stratus OCT (Carl Zeiss Meditec, Dublin, CA). In general, the recent developments of commercial devices demonstrate a trend of improving axial resolution. We have developed a 2-μm resolution OCT device that allows the visualization of fine details of the retinal structure.[12] Logically, the next step to undertake is the automatic segmentation of the high-resolution OCT images obtained with this particular device. Most algorithms within the commercial devices only provide thickness information for a small number of retinal layers, such as the RNFL and the macula. These commercial algorithms are normally not accessible due to its proprietary nature, forcing the development of independent custom-built softwares.[46] For example, Cabrera DeBuc et al. developed a custom-built software for extracting up to six intraretinal layers (including RPE) from Stratus OCT images.[16,17] Several OCT prototypes with ultra-high resolution[47–49] have demonstrated excellent hardware setups, but image processing has lagged behind. The lagging image processing may limit the use of advanced OCT devices with higher resolution, especially at the prototype stage. In the present study, the manual method for segmenting up to nine intraretinal layers in a small area nasally from the fovea was tested as a first step prior to future
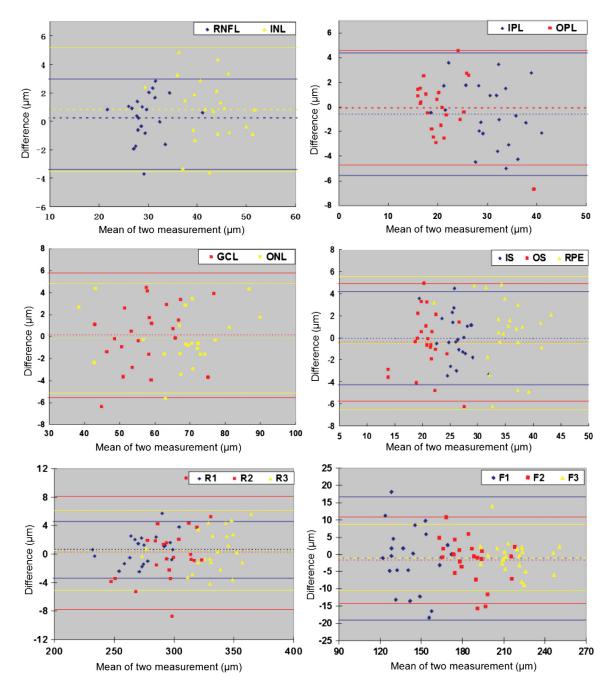
Fig. 4 Bland–Altman plots of the agreement of the two measurements of the intraretinal layers and retinal segments (including their corresponding foveal center measurements). Values on the horizontal axis correspond to the mean of the two measurements. Values on the vertical axis correspond to the difference of two measurements. The horizontal full lines represent the mean and mean ±1.96 SD. R = retina; F = fovea.

clinical studies and further development of robust automatic segmentation software. As a matter of fact, our preliminary analysis pointed the main issues that need to be addressed to obtain a fully automatic segmentation of the overall nine layers manually extracted using UHR-OCT. Even though the results presented were mainly based on manual segmentation of UHR-OCT images and only a subset of eyes was automatically segmented for comparison purposes, the main determination was to establish the repeatability of measurements by visual inspection using UHR-OCT. The agreement demonstrated in the comparison between manual and automatic segmentation methods in the subset of data may provide information on further development of the automatic segmentation software.

A more practical interface and robust algorithm to segment all intraretinal layers and handle the large quantities of measured raw data generated by our system along with the associated substantial processing are certainly required, and it is currently under development.

The results of the present study are in agreement with others, although differences exist. In general, the retinal thickness measurements obtained with various OCT systems are different.[3,50–55] The differences are due to the methods, sampling points, registration, definitions and algorithms for segmenting the boundaries of intraretinal layers.[3,50–55] OCT defines the inner retinal boundary as the ILM. There are important differences and assumptions for the location of outer retinal boundaries.
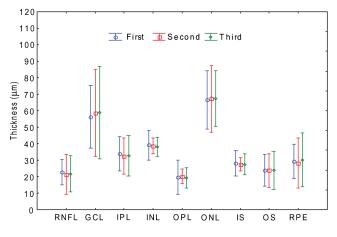
Fig. 5 Inter-session variations of manually segmented intra-retinal layers among three imaging sessions. Eight eyes of 4 subjects were imaged in three independent sessions. Three graders manually segmented all 9 intra-retinal layers. No significances were found among sessions. The results correlated well. The nine layers of the retina are: the retinal nerve fiber layer (RNFL), ganglion cell layer (GCL), inner plexiform layer (IPL), inner nuclear layer (INL), outer plexiform layer (OPL), outer nuclear layer (ONL), the photoreceptor inner segment (IS), the photoreceptor outer segment (OS), and the retinal pigment epithelium (RPE). OLM = outer limiting membrane; IS/OS = the junction of photoreceptor inner and outer segments; OS/RPE = the junction of the outer segments and RPE. Bars = 95% confidence interval.

We defined and segmented retinal layers according to assumptions used by commercial OCT instruments and other studies. We defined three retinal segments: Retina 1, Retina 2 and Retina 3. Thickness measurement calculated using the Retina 1 segment is similarly defined as in the Stratus OCT system. Retina 2 is defined in a manner similar to the Cirrus OCT and RTVue-100. Retina 3 is similar to Spectralis OCT and Topcon 3D OCT. Our results using different assumptions for
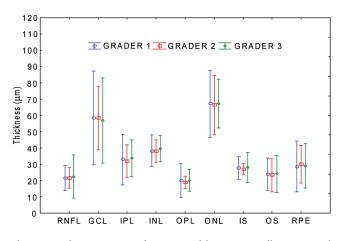

Fig. 6 Interclass variations of intra-retinal layers manually segmented by three graders. Eight eyes of 4 subjects were imaged in three independent sessions. Three graders manually segmented all 9 intra-retinal layers. No significances were found among graders. The results correlated well. The nine layers of the retina are: the retinal nerve fiber layer (RNFL), ganglion cell layer (GCL), inner plexiform layer (IPL), inner nuclear layer (INL), outer plexiform layer (OPL), outer nuclear layer (ONL), the photoreceptor inner segment (IS), the photoreceptor outer segment (OS), and the retinal pigment epithelium (RPE). OLM = outer limiting membrane; IS/OS = the junction of photoreceptor inner segment and outer segment; OS/RPE = the junction of the outer segments and RPE. Bars = 95% confidence interval.
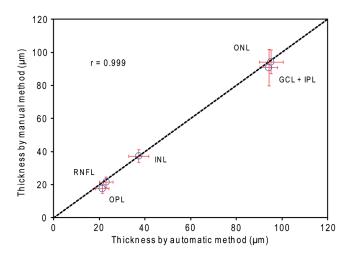

Fig. 7 Correlation between manual and automatic segmentation methods. Eight images of 8 eyes were segmented manually and automatically. The segmentation results of 5 intraretinal layers, which were automatically segmented, were compared to the manual segmentation results. Both results appeared to correlate well. The dash line represents the equality. Bars = standard deviation.

the outer border of the retina were very similar to those from images obtained with these commercial devices. Different definitions for the retinal thickness yield different thickness of the retina and apparently different repeatability as evident in our results. In addition, the repeatability of the total retinal thickness was linked to the contributing boundaries that formed the layer. Retina 1 with the assumption using the IS/OS junction as outer border provided a much better repeatability and Retina 2 gave the worst repeatability. It may be necessary to take into account the definition of the outer boundary and the characteristics of the contrast transition between the layers and structures at each side of the border used as the outer border of the retina.

The mean foveal thickness (Fovea 1) was approximately 140 μm in the present study, which was thinner than that measured by Hee et al. (152 μm)[56] and Paunescu et al. (169 μm).[24] Hee et al. defined the retina between the ILM and the anterior border of IS/OS junction as observed from their figures. Paunescu et al. used Stratus OCT for the measurement. Huang et al.[52] used software calipers to measure the distance from the ILM to the IS/OS junction at the center point of the fovea in RTVue images. The thickness was 141 μm, which matched our calculations. Race also affects the macular thickness. Asian and black subjects have thinner maculas compared with white subjects.[7,57] The subjects in the present study and that of Huang et al.'s were Asians, and both studies found thinner maculas. Our total retinal thickness (Retina 1) was in good agreement with the findings of Koozekanani et al. who measured the retinal thickness as 274 μm over a similar region.[58] It may not be comparable to others who used a different region for calculating the total retinal thickness. The cup-to-disc ratio was also found similar to Paunescu et al.'s study.[24]

Although manual grading of intraretinal layers is time consuming, it may provide some advantage for repeatability testing. Commercial and custom software, such as the one used by Cabrera DeBuc et al.,[15–17] often requires manual correction of segmentation failure, which may not be necessarily related to the accuracy of the measurement.[16,17,54] Segmentation algorithms used in OCT reading centers often require visual inspection after automatic segmentation. Ho et al.[59] assessed the artifacts

of several commercial OCT devices (Stratus OCT, Cirrus OCT, RTVue-100, and Topcon 3D-OCT 1000). Time domain OCT, such as Stratus OCT, may have improper central foveal thickness after manual correction compared with spectral domain OCT.[59] Spectral domain OCT devices such as Cirrus were found to have the lowest occurrence of artifacts, improper central foveal thickness, and clinically improper central foveal thickness. The repeatability of our method appeared reasonably good. Good retinal CRs may represent the ultra-high resolution of our system.[17] Using Stratus OCT, Polito et al. demonstrated that the CR of the macula varied[60] between 1.68% and 7.43%. With a similar study design and sample size, Paunescu et al. reported that the ICC of the total and regional macular thickness measurements ranged between 0.55 and 0.97.[24] Leung et al. also observed relatively good repeatability for Stratus OCT macular thickness measurements.[3] The ICC was reported from 0.85 to 0.91. Using spectral domain OCT, they found that the measurement repeatability was even better.[3] They explained that the better repeatability may be attributable to the higher scan rate and the increased sampling frames in the spectral domain OCT. Hangai M. et al. tested automated segmentation of multiple intraretinal layers from a 3-dimensional spectral domain OCT, the reproducibility of measurements of single and combined layers were assessed (M., Hangai et al., IOVS 2010;51:

ARVO E-abstract 221). Significant detection failure was evident, and the ICC of some detected layers like IPL, IS, OS and RPE was not as good as that measured in the present study.

There are some limitations to the present study. First, the sample size of subjects was relatively small. A larger sample size is necessary to fully test the sensitivity and specificity of our method. We attempted to test the repeatability of thickness measurements of intraretinal layers, which were found to be close to the results previously reported.[16,17] Second, it lacked a reliable OCT gold standard of the retinal thickness, particularly for these intraretinal layers. Third, manually outlining the boundaries and performing calculations were time consuming, which limits its use in large-scale clinical studies. Fourth, our UHR-OCT device can scan 3D datasets but 2D images were segmented in the present study. Further development of thickness maps of intraretinal layers will be performed.

In conclusion, our results showed that more intraretinal layers are imageable with ultra-high resolution OCT. The image can be segmented to measure these visualized layers with reasonably good repeatability. Future development of three dimensional rending and robust segmentation software will be needed to test diagnostic values in diseased eyes.

Table 1 Averaged thickness measurements (mean ± SD) per scanning session, mean thickness values (mean ± SD) calculated from the two scanning session's data, coefficients of repeatability, and intraclass correlation coefficients obtained for retinal segments (including their corresponding foveal center measurements) and nine intraretinal layers shown in Fig. 1. Results were obtained after scanning twice (Sessions 1 and 2) 23 eyes of the 12 subjects under the same conditions by one examiner.

	Thickness (μm)				ICC	CR(μm)	CR (%)
	Session 1	Session 2	Mean	Difference			
RNFL	29.4 ± 3.6	29.6 ± 3.9	29.5 ± 3.7	0.23	0.952	3.24	11.00
GCL	57.8 ± 8.6	57.9 ± 9.5	57.9 ± 9.0	0.13	0.974	5.79	10.01
IPL	30.8 ± 6.4	30.2 ± 5.7	30.5 ± 5.9	−0.57	0.954	5.07	16.62
INL	42.3 ± 6.0	43.1 ± 5.4	42.7 ± 5.6	0.81	0.961	4.42	10.36
OPL	21.0 ± 5.8	20.9 ± 4.8	21.0 ± 5.2	−0.04	0.948	4.72	22.53
ONL	67.7 ± 12.7	67.5 ± 12.7	67.6 ± 12.7	−0.17	0.990	5.07	7.50
IS	26.3 ± 3.1	26.4 ± 2.4	26.3 ± 2.6	0.06	0.824	4.31	16.37
OS	21.1 ± 3.4	20.6 ± 3.4	20.8 ± 3.1	−0.44	0.808	5.46	26.20
RPE	34.9 ± 5.0	35.4 ± 4.4	35.1 ± 4.5	0.51	0.881	6.15	17.53
RETINA1	275.3 ± 19.2	275.9 ± 19.8	275.6 ± 19.5	0.62	0.997	4.06	1.47
RETINA2	296.3 ± 20.5	296.5 ± 22.3	296.4 ± 21.3	0.19	0.991	8.09	2.73
RETINA3	331.2 ± 22.1	331.7 ± 22.8	331.4 ± 22.4	0.52	0.996	5.71	1.72
FOVEA1	144.0 ± 17.0	142.7 ± 15.2	143.3 ± 15.4	−1.21	0.912	18.30	12.77
FOVEA2	187.3 ± 17.3	185.6 ± 14.9	186.4 ± 15.9	−1.73	0.959	12.77	6.85
FOVEA3	218.2 ± 16.4	217.2 ± 15.0	217.7 ± 15.5	−0.96	0.975	9.80	4.50
	Cup-to-disc ratio						
C/D	0.51 ± 0.26	0.51 ± 0.27	0.51 ± 0.26	−0.001	0.999	0.03	6.21

References

1. D. Huang et al., "Optical coherence tomography," *Science* **254**(5035), 1178–1181 (1991).
2. E. Garcia-Martin et al., "Intra and interoperator reproducibility of retinal nerve fibre and macular thickness measurements using Cirrus Fourier-domain OCT," *Acta Ophthalmol.* **89**(1), e23–e29 (2011).
3. C. K. Leung et al., "Comparison of macular thickness measurements between time domain and spectral domain optical coherence tomography," *Invest. Ophthalmol. Vis. Sci.* **49**(11), 4893–4897 (2008).
4. C. A. Puliafito et al., "Imaging of macular diseases with optical coherence tomography," *Ophthalmology* **102**(2), 217–229 (1995).
5. A. Petzold et al., "Optical coherence tomography in multiple sclerosis: a systematic review and meta-analysis," *Lancet Neurol.* **9**(9), 921–932 (2010).
6. S. Saidha et al., "Primary retinal pathology in multiple sclerosis as detected by optical coherence tomography," *Brain* **134**(2), 518–533 (2011).
7. V. Guedes et al., "Optical coherence tomography measurement of macular and nerve fiber layer thickness in normal and glaucomatous human eyes," *Ophthalmology* **110**(1), 177–189 (2003).
8. M. Wojtkowski et al., "Ultrahigh-resolution, high-speed, Fourier domain optical coherence tomography and methods for dispersion compensation," *Opt. Express* **12**(11), 2404–2422 (2004).
9. M. Wojtkowski et al., "Three-dimensional retinal imaging with high-speed ultrahigh-resolution optical coherence tomography," *Ophthalmology* **112**(10), 1734–1746 (2005).
10. M. A. Shousha et al., "Use of ultra-high-resolution optical coherence tomography to detect in vivo characteristics of Descemet's membrane in Fuchs' dystrophy," *Ophthalmology* **117**(6), 1220–1227 (2010).
11. Q. Chen et al., "Ultrahigh-resolution measurement by optical coherence tomography of dynamic tear film changes on contact lenses," *Invest Ophthalmol. Vis. Sci.* **51**(4), 1988–1993 (2010).
12. D. Zhu et al., "Broadband superluminescent diode-based ultrahigh resolution optical coherence tomography for ophthalmic imaging," *J. Biomed. Opt.* **16**(12), 126006 (2011).
13. H. Jiang et al., "Slit-lamp-adapted ultra-high resolution OCT for imaging the posterior segment of the eye," *Ophthalmic Surg. Laser. Imag.* **43**(1), 76–81 (2012).
14. D. C. Fernandez and H. M. Salinas, "A tissue phantom for investigating volume quantification on retinal images obtained with the Stratus OCT system," in *Proc. 26th Annual Int. Conf. of the IEEE Engineering in Medicine and Biology* Vol. **1**(1), pp. 1225–1228, EMBS, Piscataway, NJ, USA (2004).
15. E. Tatrai et al., "In vivo evaluation of retinal neurodegeneration in patients with multiple sclerosis," *PLoS. One.* **7**(1), e30922 (2012).
16. D. C. Debuc et al., "Reliability and reproducibility of macular segmentation using a custom-built optical coherence tomography retinal image analysis software," *J. Biomed. Opt.* **14**(6), 064023 (2009).
17. D. C. Debuc et al., "Improving image segmentation performance and quantitative analysis via a computer-aided grading methodology for optical coherence tomography retinal image analysis," *J. Biomed. Opt.* **15**(4), 046015 (2010).
18. E. Tatrai et al., "Comparison of retinal thickness by Fourier-domain optical coherence tomography and OCT retinal image analysis software segmentation analysis derived from Stratus optical coherence tomography images," *J. Biomed. Opt.* **16**(5), 056004 (2011).
19. D. T. Miller et al., "Adaptive optics and the eye (super resolution OCT)," *Eye (Lond)* **25**(3), 321–330 (2011).
20. M. F. Marmor et al., "Visual insignificance of the foveal pit: reassessment of foveal hypoplasia as fovea plana," *Arch. Ophthalmol.* **126**(7), 907–913 (2008).
21. G. S. Hageman et al., "The interphotoreceptor matrix mediates primate retinal adhesion," *Arch. Ophthalmol.* **113**(5), 655–660 (1995).
22. B. Povazay et al., "Wide-field optical coherence tomography of the choroid in vivo," *Invest Ophthalmol. Vis. Sci.* **50**(4), 1856–1863 (2009).
23. B. Sander et al., "Enhanced optical coherence tomography imaging by multiple scan averaging," *Br. J. Ophthalmol.* **89**(2), 207–212 (2005).
24. L. A. Paunescu et al., "Reproducibility of nerve fiber thickness, macular thickness, and optic nerve head measurements using StratusOCT," *Invest Ophthalmol. Vis. Sci.* **45**(6), 1716–1724 (2004).
25. H. L. Rao et al., "Predictors of normal optic nerve head, retinal nerve fiber layer, and macular parameters measured by spectral domain optical coherence tomography," *Invest Ophthalmol. Vis. Sci.* **52**(2), 1103–1110 (2011).
26. J. M. Bland and D. G. Altman, "Statistical methods for assessing agreement between two methods of clinical measurement," *Lancet* **327**(8476), 307–310 (1986).
27. J. J. Bartko and W. T. Carpenter Jr., "On the methods and theory of reliability," *J. Nerv. Ment. Dis.* **163**(5), 307–317 (1976).
28. S. Fukuda et al., "Repeatability and reproducibility of anterior chamber volume measurements using 3-dimensional corneal and anterior segment optical coherence tomography," *J. Cataract Refract. Surg.* **37**(3), 461–468 (2011).
29. S. Mohamed et al., "Repeatability and reproducibility of pachymetric mapping with Visante anterior segment-optical coherence tomography," *Invest Ophthalmol. Vis. Sci.* **48**(12), 5499–5504 (2007).
30. M. Siger et al., "Optical coherence tomography in multiple sclerosis: thickness of the retinal nerve fiber layer as a potential measure of axonal loss and brain atrophy," *J. Neurol.* **255**(10), 1555–1560 (2008).
31. E. Gordon-Lipkin et al., "Retinal nerve fiber layer is associated with brain atrophy in multiple sclerosis," *Neurology* **69**(16), 1603–1609 (2007).
32. U. Ziemann et al., "Development of biomarkers for multiple sclerosis as a neurodegenerative disorder," *Prog. Neurobiol.* **95**(4), 670–685 (2011).
33. T. D. Ko et al., "Ultrahigh resolution optical coherence tomography imaging with a broadband superluminescent diode light source," *Opt. Express* **12**(10), 2112–2119 (2004).
34. R. Leitgeb et al., "Ultrahigh resolution Fourier domain optical coherence tomography," *Opt. Express* **12**(10), 2156–2165 (2004).
35. N. Nassif et al., "In vivo human retinal imaging by ultrahigh-speed spectral domain optical coherence tomography," *Opt. Lett.* **29**(5), 480–482 (2004).
36. N. Nassif et al., "In vivo high-resolution video-rate spectral-domain optical coherence tomography of the human retina and optic nerve," *Opt. Express* **12**(3), 367–376 (2004).
37. M. Mujat et al., "High resolution multimodal clinical ophthalmic imaging system," *Opt. Express* **18**(11), 11607–11621 (2010).
38. R. J. Zawadzki et al., "Adaptive optics-optical coherence tomography: optimizing visualization of microscopic retinal structures in three dimensions," *J. Opt. Soc. Am. A Opt. Image Sci. Vis.* **24**(5), 1373–1383 (2007).
39. M. Wojtkowski et al., "Three-dimensional retinal imaging with high-speed ultrahigh-resolution optical coherence tomography," *Ophthalmology* **112**(10), 1734–1746 (2005).
40. A. W. Scott et al., "Imaging the infant retina with a hand-held spectral-domain optical coherence tomography device," *Am. J. Ophthalmol.* **147**(2), 364–373 (2009).
41. M. T. Leite et al., "Comparison of the Diagnostic Accuracies of the Spectralis, Cirrus, and RTVue Optical Coherence Tomography Devices in Glaucoma," *Ophthalmology* **118**(7), 1334–1339 (2011).
42. N. Maeda, "Optical coherence tomography for corneal diseases," *Eye Contact Lens* **36**(5), 254–259 (2010).
43. J. L. Fine et al., "Direct scanning of pathology specimens using spectral domain optical coherence tomography: a pilot study," *Ophthalmic Surg. Laser. Imag.* **41** Suppl, S58–S64 (2010).
44. P. Godara et al., "Assessing the photoreceptor mosaic over drusen using adaptive optics and SD-OCT," *Ophthalmic Surg. Laser. Imag.* **41** Suppl, S104–S108 (2010).

45. J. M. Gonzalez-Meijome et al., "High-resolution spectral domain optical coherence tomography technology for the visualization of contact lens to cornea relationships," *Cornea* **29**(12), 1359–1367 (2010).

46. D. C. DeBuc, "A review of algorithms for segmentation of retinal image data using optical coherence tomography" in *Image Segmentation*, P. G. Ho, ed., InTech, Rijeka, Croatia (2011).

47. M. Ruggeri et al., "In vivo three-dimensional high-resolution imaging of rodent retina with spectral-domain optical coherence tomography," *Invest Ophthalmol. Vis. Sci.* **48**(4), 1808–1814 (2007).

48. M. Wojtkowski et al., "Three-dimensional retinal imaging with high-speed ultrahigh-resolution optical coherence tomography," *Ophthalmology* **112**(10), 1734–1746 (2005).

49. W. Drexler et al., "Ultrahigh-resolution ophthalmic optical coherence tomography," *Nat. Med.* **7**(4), 502–507 (2001).

50. F. Forooghian et al., "Evaluation of time domain and spectral domain optical coherence tomography in the measurement of diabetic macular edema," *Invest Ophthalmol. Vis. Sci.* **49**(10), 4290–4296 (2008).

51. A. Giani et al., "Reproducibility of retinal thickness measurements on normal and pathologic eyes by different optical coherence tomography instruments," *Am. J. Ophthalmol.* **150**(6), 815–824 (2010).

52. J. Huang et al., "Macular thickness measurements in normal eyes with time-domain and Fourier-domain optical coherence tomography," *Retina* **29**(7), 980–987 (2009).

53. M. T. Leite et al., "Agreement among spectral-domain optical coherence tomography instruments for assessing retinal nerve fiber layer thickness," *Am. J. Ophthalmol.* **151**(1), 85–92 (2011).

54. S. R. Sadda et al., "Error correction and quantitative subanalysis of optical coherence tomography data using computer-assisted grading," *Invest Ophthalmol. Vis. Sci.* **48**(2), 839–848 (2007).

55. U. E. Wolf-Schnurrbusch et al., "Macular thickness measurements in healthy eyes using six different optical coherence tomography instruments," *Invest Ophthalmol. Vis. Sci.* **50**(7), 3432–3437 (2009).

56. M. R. Hee et al., "Topography of diabetic macular edema with optical coherence tomography," *Ophthalmology* **105**(2), 360–370 (1998).

57. B. Asefzadeh, A. A. Cavallerano, and B. M. Fisch, "Racial differences in macular thickness in healthy eyes," *Optom. Vis. Sci.* **84**(10), 941–945 (2007).

58. D. Koozekanani et al., "Intersession repeatability of macular thickness measurements with the Humphrey 2000 OCT," *Invest Ophthalmol. Vis. Sci.* **41**(6), 1486–1491 (2000).

59. J. Ho et al., "Assessment of artifacts and reproducibility across spectral- and time-domain optical coherence tomography devices," *Ophthalmology* **116**(10), 1960–1970 (2009).

60. A. Polito et al., "Repeatability and reproducibility of fast macular thickness mapping with stratus optical coherence tomography," *Arch. Ophthalmol.* **123**(10), 1330–1337 (2005).